Proceedings of the SEM Annual Conference
June 7-10, 2010 Indianapolis, Indiana USA

A Test Platform for Systematic Investigation of Tribology in MEMS

N. Ansari[a,*] and W. R. Ashurst[a]
[a]Department of Chemical Engineering, Auburn University, Auburn, AL 36849 USA
*Corresponding author: ansarna@auburn.edu (N. Ansari)

Abstract

Tribology remains an active area of research for the Micro-electromechanical Systems (MEMS) community. At the micron scale, which is the scale relevant to commercial MEMS, a number of factors namely roughness, apparent contact area, surface topography, surface chemistry, etc. are known to have a significant impact on the tribological properties. Historically, researchers have found it difficult to study the effects of these factors individually. We report on a test platform designed and fabricated using a single mask scheme within a relatively smooth SOI wafer. The test platform includes several different micromechanisms on the same chip so that a systematic investigation of the factors that influence tribology in MEMS can be carried out. The test platform is therefore an ideal stage for testing and comparing the various strategies that can be used to address the tribological issues that are presently plaguing the MEMS community.

1. Introduction

In the micro-domain, tribology is influenced by several factors, only some of which are known. Taller asperities being the real points of contact between two surfaces, the real area of contact between them is determined by their roughness, material properties and the shapes of asperities on them. Roughness and topography of contacting surfaces therefore have a strong influence on tribology [1–3]. Both of these factors have their origins in grain orientation and processes used in the fabrication of MEMS, as a result of which, we have very limited control over them [4]. The chemical compositions of the contacting surfaces are also known to have a significant influence on tribology. For example, a hydrophobic surface with a relatively low surface energy is less prone to adhesion [5–7]. Also, environmental factors like high relative humidity can lead to capillary condensation in narrow gaps between hydrophilic surfaces, thereby, making them more prone to adhesion [3]. Studying the effects of each of these factors individually is therefore critical for a precise understanding of tribology.

Historically, the test platforms used to investigate tribology are fabricated using polysilicon structural layers. The inherent roughness of the in-plane (rms roughness is 4.91 nm) and sidewall (rms roughness is 13.8 nm) surfaces of polysilicon structural layers is evident in the AFM images shown in Fig. 1a and Fig. 1b. Further, linescans across these AFM images, shown in Fig. 1a and Fig. 1b indicate that both the in-plane as well as sidewall polysilicon surfaces have significantly high peak to valley ratio. As a result, researchers have found it difficult to study the effects of factors influencing tribology individually since the effects of inherent roughness of the polysilicon structural layers is always coupled with the effects of other factors. Additionally, the material properties of the polysilicon structural layers vary from fabrication to fabrication and sometimes even from chip to chip. Properties like residual stress, Young's modulus and stress gradient are extremely sensitive to the deposition and annealing conditions of polysilicon structural layers and hence these properties sometimes even vary on the same chip [8, 9].

2. The Test Platform

In order to address these issues of inherent roughness and inconsistent material properties of polysilicon structural layers used in conventional test platforms, we have designed a single mask scheme to fabricate a test platform within an SOI wafer. The structural layer of our test platform is a 2 μm thin film of Si(100) on top of a 500 μm thick Si(100) substrate. A 2 μm thin sacrificial BOX oxide is sandwiched between the substrate and the structural layer. Since the substrate and the device layer are both single crystal silicon surfaces, they are relatively much smoother than the polysilicn structural layers used in conventional test platforms. This is clearly evident from the AFM image of the in-plane surface (rms roughness is 0.097 nm) of the test platform reported in this paper, shown in Fig. 2a. A linescan

T. Proulx (ed.), *MEMS and Nanotechnology, Volume 2*, Conference Proceedings of the Society for Experimental Mechanics Series 2,
DOI 10.1007/978-1-4419-8825-6_14, © The Society for Experimental Mechanics, Inc. 2011

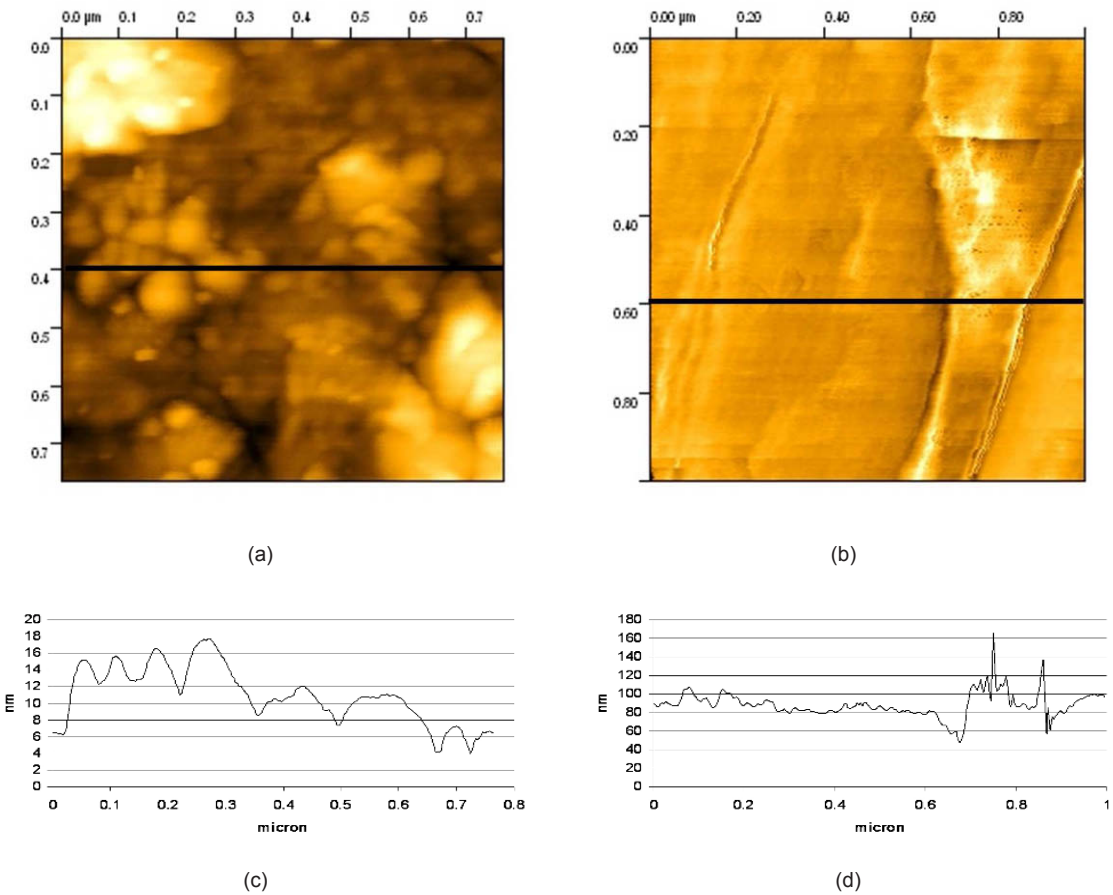

Figure 1: (a) AFM image of an in-plane polysilicon surface (b) AFM image of a sidewall polysilicon surface (c) Linescan across image a (d) Linescan across image b)

across this AFM image of the in-plane surface shows significantly reduced peak to valley ratio. It must be noted that a large fraction of this already small peak to valley ratio is due to the inherent noise of the AFM. The sidewall surface (rms roughness is 6.52 nm) of the test platform reported in this paper has a peak to valley ratio higher than that of its in-plane surface, but it is still lesser than that of a polysilicon sidewall surface. Also, the material properties of single crystal silicon surfaces do not vary much. Furthermore, to eliminate the inconsistencies resulting from the fabrication process variations, the test platform includes several different micromechanisms so that a complete systematic investigation of all the tribological properties can be carried out on the same chip.

The Test Platform (TP) reported in this paper is fabricated using a single mask scheme and hence is facile and inexpensive to fabricate. Also, the time required to fabricate TP is significantly lesser than that required to fabricate most of the conventional test platforms. In essence, TP is an extremely useful and versatile tool, which on one hand saves a lot of time and money while on the other hand facilitates a systematic investigation of several tribological properties critical to MEMS. TP has micromechanisms that can be used to determine several material properties like the residual stress in a released structural layer. The fracture strength and the Young's modulus of the structural layer can also be determined.

Conventionally, most of the adhesion studies are conducted on in-plane surfaces although, it is the sidewall surfaces that often come into contact in most useful MEMS. Additionally, it is clearly evident from the AFM images shown in Fig. 2a and Fig. 2b that the in-plane and sidewall surfaces are significantly different topographically. They are also expected to be different chemically. These differences are a result of different processing environments to which these surfaces have been exposed during fabrication. Since the in-plane and sidewall surfaces are topographically

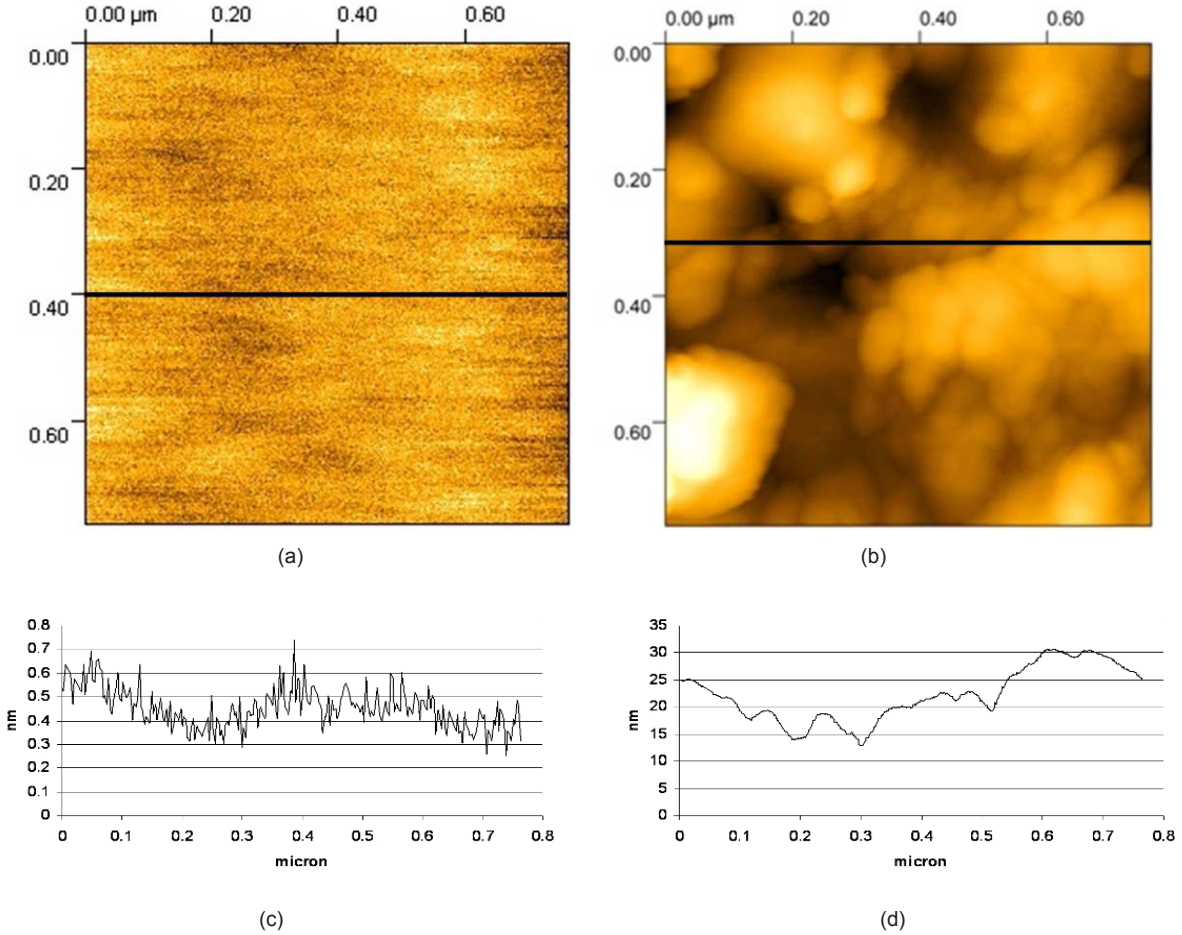

Figure 2: (a) AFM image of an in-plane surface of the test platform(b) AFM image of a sidewall surface of the test platform (c) Linescan across image a (d) Linescan across image b

and chemically different, different microinstruments are needed to study tribology between them. TP conveniently addresses this need. It has microinstruments to study adhesion between both in-plane as well as sidewall surfaces. It also has three different microinstruments that can be used to study and compare friction and wear between sidewall surfaces.

3. Microinstruments

3.1 Material Properties

TP has microinstruments that can be used to determine certain material properties of the structural film. Figure 3a is an optical image of a Residual Stress Tester (RST), which when released can be used to determine the residual stress in the structural film. Depending on the nature of residual stress in the structural film (i.e., tensile or compressive), the suspended beam shown in Fig. 3a either rotates clockwise or anti-clockwise respectively on getting released. By optically matching the patterns shown in Fig. 3b, the rotation (θ) of the released suspended beam can be accurately determined. The residual stress (σ_R) in the released structural film is determined using Eq. 1, where z is a constant that depends on the material properties of the structural film and the physical dimensions of the suspended beam, w is the width of the supporting suspension beams that connect the suspended beam to the anchors, t is the thickness of the structural film and d as shown in Fig. 3a is the distance between the two supporting suspension beams.

$$\sigma_R = z(\frac{\theta}{wtd}) \tag{1}$$

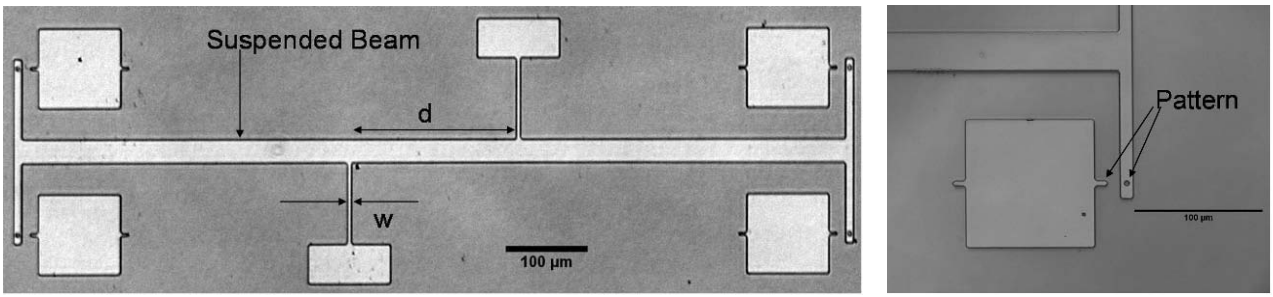

(a) (b)

Figure 3: (a) Optical image of the Residual Stress Tester (b) Magnified optical image showing patterns that are used for pattern matching

The Mechanical Strength Tester (MST) shown in Fig. 4a can be used to determine the fracture strength of the structural film. The shuttle, which is suspended using four suppporting beams is pushed in the direction indicated by the arrow in Fig. 4a using a Signatone SE-20T probe tip, which is controlled using an open loop peizo. As the displacement of the shuttle increases, the beams that are protruding out of the shuttle are pushed against the anchored stopper blocks until they break-off from the shuttle. Optical pattern matching is used to determine the displacement of the shuttle. The fracture strength (σ_{max}) of the structural film is calculated using Eq. 2, where E is the Young's modulus of the structural film, w is the width of the fractured beam, δ is the distance by which the shuttle is displaced when the beam gets fractured and L_c is the distance between the suttle and the anchored stoppers. Each MST has three sets of two beams each with each set of beams having a different length than the other two sets.

$$\sigma_{max} = \frac{3Ew\delta}{2L_c^2} \tag{2}$$

Young's modulus (E), which is one of the most critical material properties of the structural film, can be determined using the resonators. The resonators are actuated elecrostatically by applying an AC voltage across one set of comb fingers and grounding the other set of comb fingers as well as the suspended resonating structure. Resonance is determined optically with an accuracy of $\pm$ 10 Hz. The resonance frequency (f_R) of a resonator is given by the Rayleigh equation (i.e., Eq. 3 given below), where k_x is the stiffness of the folded suspension beams supporting the resonating structure and it depends on E of the structural film and the true dimensions of the folded supporting suspension beams and M_{eff} is the effective mass of the resonating structure. The rearranged form of the Rayleigh

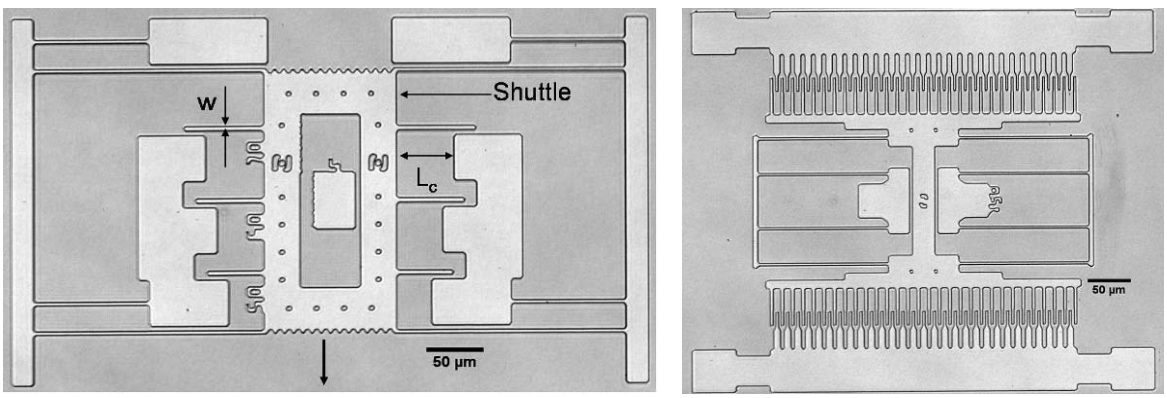

(a) (b)

Figure 4: (a) Optical image of the Mechanical Strength Tester (b) Optical image of a Resonator

equation given by Eq. 4 can be used to extract the Young's modulus of the structural film, where t is the thickness of the structural film and w and L are width and length of the folded suspension supporting beams respectively. TP has resonators with seven different folded suspension beam lengths and there are multiple copies of each one of them.

$$f_R = \frac{1}{2\pi}\sqrt{\frac{k_x}{M_{eff}}} \tag{3}$$

$$f_R^2 = (\frac{tw^3}{2\pi^2 M_{eff} L^3})E \tag{4}$$

3.2 Adhesion

Apparent work of adhesion ($\mathcal{W}_{ip}$) between in-plane surfaces can be accurately determined using the Cantilever Beam Array (CBA) shown in Fig. 5a. Each beam in the array is actuated manually by pushing it with a sharp tungsten probe tip until it contacts the substrate, after which the probe tip is retracted carefully and slowly, which causes the beam to peel apart up to a certain characteristic length called as the crack length (s). The crack length depends on the interfacial properties of the two contacting surfaces. The crack length of each actuated beam is determined optically

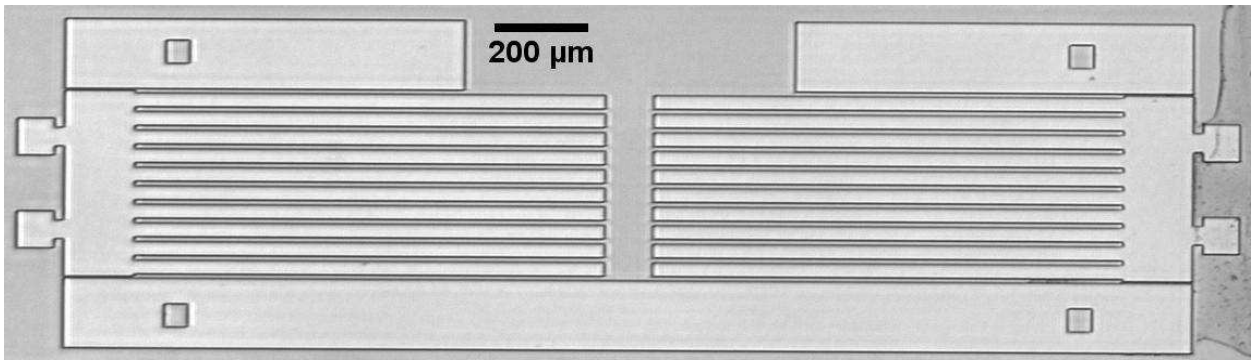

(a)

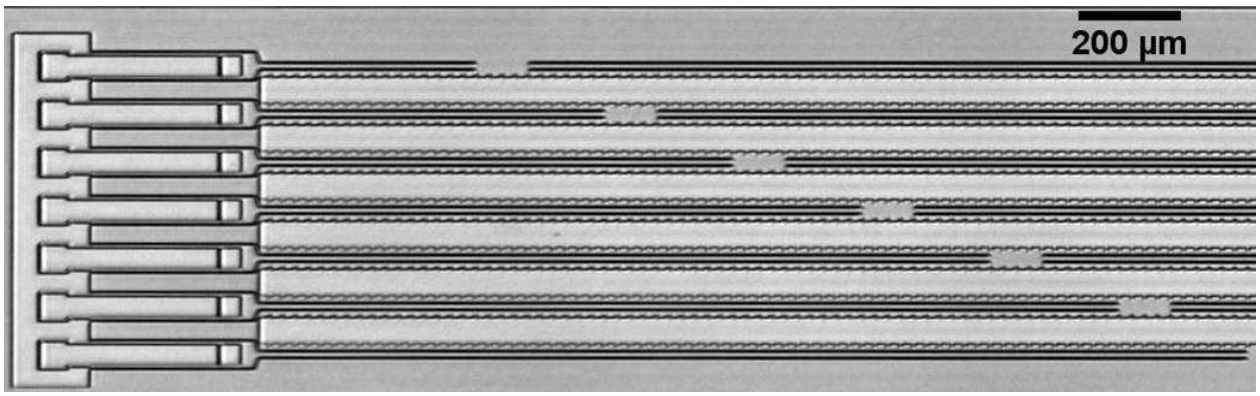

(b)

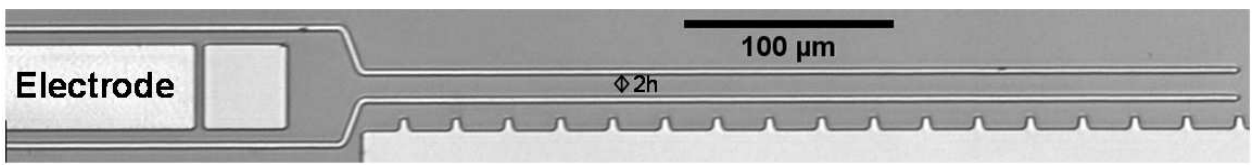

(c)

Figure 5: (a) Optical image of a Cantilever Beam Array (b) Optical image of a Sidewall Beam Array (c) Magnified optical image of a single pair of sidewall beams

using interferometry. Apparent work of adhesion between the substrate and the bottom surface of the structural film can be determined using Eq. 5 suggested by Hurst et. al., where E and t are the Young's modulus and thickness of the structural film respectively, s is the crack length and a_1 and a_2 are parameters extracted from the fitted height profile of the actuated cantilever beam, which is obtained eperimentally using phase shifting interferometry [10]. Instead of cantilever beams with increasing lengths, the CBA's in TP have 10 cantilever beams each, all of the same length. This allows estimation of 10 distinct data points from each CBA, which not only saves a lot of space on TP but also enables a statistical analysis of the local adhesion. To preferentially use S-shaped cantilever beams, which provide a more accurate estimation of $\mathcal{W}_{ip}$ for determining $\mathcal{W}_{ip}$ between most of the available in-plane surfaces, TP has three sets of eight CBA's each. The lengths of cantilever beams in those three sets are 500 μm, 1000 μm and 2000 μm respectively.

$$\mathcal{W}_{ip} = \frac{3Et^2}{2s^4}\left(a_1^2 + a_1 a_2 + \frac{1}{3}a_2^2\right) \tag{5}$$

The Sidewall Beam Array (SBA) shown in Fig. 5b can be used to determine the apparent worh of adhesion between sidewall surfaces ($\mathcal{W}_s$). There are 8 SBA's in TP and each one of them has seven sidewall beam pairs. The shortest sidewall beam pair has a length of 750 μm and each successive sidewall beam pair is 250 μm longer.

$$\mathcal{W}_s = \frac{3Et^3h^2}{s^4} \tag{6}$$

Each sidewall beam pair is actuated electrostatically. A DC voltage is applied to the electrode shown in Fig. 5c, while the sidewall beams and the substrate are grounded. As the voltage applied to the electrode is increased from 0 V at a rate of 1 V/s, the two sidewall beams are drawn together like tweezers. At 90 V, which is the maximum voltage applied, the beams are in contact over much of their lengths, leaving a length of about 150 μm near the electrode. The actuation voltage is then ramped down to 0 V at 1 V/s and the beams are observed to peel apart up to a certain characteristic length called as the crack length (s), which depends on the interfacial properties of the two contacting surfaces. Aapparent work of adhesion between sidewall surfaces is determined using Eq. 6, where E is the Young's modulus of the structural film, t is the width of a sidewall beam, h is half the distance between the unactuated sidewall beam pair and s is the crack length which is determined optically [7]. It should be noted that both the CBA and SBA only determine the apparent work of adhesion between contacting surfaces since all the contacting surfaces have a finite roughness and topography.

3.3 Friction

The device shown in Fig. 6a is a Sidewall Adhesion and Friction Tester (SFAT), which is a modified version of the device used by Timpe et. al. [11]. The SFAT ia a very versatile tool, which can be used to study static as well as dynamic friction between sidewall surfaces. It can also be used to study adhesion as well as wear between sidewall surfaces. It is actuated electrostatically. The substrate, suspended structures in both the arms and the unused set of comb fingers are grounded. By applying a DC voltage across one of the two sets of comb fingers in the normal arm, the normal arm is either loaded onto the contact block that protrudes out of the tangential arm or is pulled away from it. Similarly, by applying a DC voltage to one of the two sets of comb fingers in the tangential arm, the tangential can be rubbed against the normal arm.

$$\mu_s = \frac{F_f}{F_n} \tag{7}$$

Figure 6b is an optical image of another type of friction tester called as the Sidewall Friction Tester (SFT), which can also be used to study static friction, dynamic friction and wear between sidewall surfaces. The SFT is also actuated electrostatically in the same manner as the SFAT. However, unlike the contacting sidewall surfaces of SFAT, which are plane surfaces, the contacting sidewall surfaces in SFT are a pair of a plane and a cylindrical surface. The normal arm in the SFT loads a suspended beam structure onto an anchored post structure and the tangential arm slides the beam against the post. By appropriately pre-caliberating the normal and tangential arms in both the SFAT and SFT, the normal force F_n as well as the tangential force F_f applied by the two arms respectively at the onset of slip between

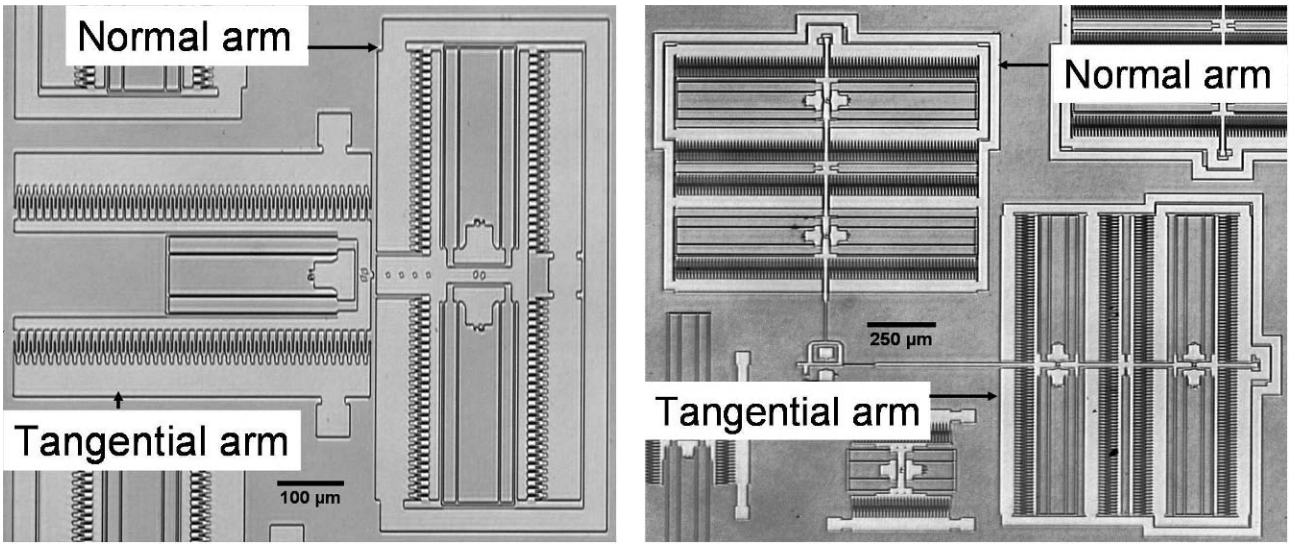

(a) (b)

Figure 6: (a) Optical image of a Sidewall Adhesion and Friction Tester (b) Optical image of a Sidewall Friction Tester

the contacting sidewall surfaces can be accurately determined. The onset of slip is detected optically using a pattern matching technique and the coefficient of static friction (μ_s) is calculated using Eq. 7.

4. Fabrication and Testing procedure of Microinstruments

Standard surface micromachining technology is used to fabricate the TP. Since the TP is fabricated within an SOI wafer, which has only one structural layer, it can be fabricated using a single mask scheme. In addition to avoiding the errors associated with mask misallignment and making the fabrication procedure extremely facile, the single mask scheme designed by us also makes it extremely inexpensive. The fabricated TP is released by etching in a solution of conc. HF (49 wt.%). After all the microinstruments on the TP are released, the etchant is completely rinsed away with deionized (DI) water. The TP is then placed in hot H_2O_2 (75-80 $^\circ$C) for 10 min. for oxidizing the test surfaces after which it is rinsed with DI water again.

Two types of surfaces are studied in this paper, namely hydrophobic surfaces coated with OTS SAM coating and hydrophilic surfaces having only native oxide on them. To obtain test surfaces having only native oxide on them, DI water is rinsed away with isopropanol (IPA) and the TP is supercritically dried in a Tousimis Autosamdri 815-B CPD system. Samples dried in this CPD system are known to have contaminated surfaces. In order to clean the test surfaces before testing, the TP is treated with a low power (25 W), capacitively coupled RF (13.56 Mhz) plasma of oxygen (O_2 pressure used is 300 mtorr). This treatment results in clean and oxidized test surfaces, including surfaces underneath the microinstruments. Water Contact angle measured on a simultaneously processed Si(100) test chip after this treatment is found to be $<5^\circ$, indicating that the treated surfaces are hydrophilic. The TP is actuated immediately after plasma cleaning to minimize contamination from the ambient. To obtain test surfaces coated with OTS SAM coating, IPA is further rinsed away with anhydrous hexane. The TP is then transferred into a conditioned OTS coating solution in a glass dish which had been previously treated with OTS. After 45 mins, the TP is transferred back to pure anhydrous hexane, which is subsequently displaced with IPA and the IPA is similarly displaced with DI water. The TP is then removed from DI water in one, slow but continuous motion in such a way that its in-plane surfaces are perpendicular to the liquid surface. All the solvent displacements are carried out using a fill/drain approach suggested by Ashurst et. al. [7]. After this treatment, the water contact angle on a simultaneously processed Si(100) test chip is measured to be 108°, indicating that the treated surfaces are hydrophobic.

Electrical contacts to the microinstruments are made by touching the actuation pads (fabricated in the microinstruments) with sharp tungsten probe tips. Interferometry using monochromatic green light (532 nm) is employed to determine the out-of-plane height profile.

5. Results and Discussion

In order to test the validity of the performance of the TP, the performance is tested on two different chips. The test surfaces on one of the chips (referred as chip A) are coated with OTS SAM coating and the test surfaces on the other chip (referred as chip B) have only native oxide on them. The tribological properties of these two types of surfaces are considered as benchmarks by the MEMS community. The following sections will individually discuss the performance of the different microinstruments on the test platform.

5.1 Material Properties

For both chip A and chip B, optical images of the RST are collected before and after releasing it. By applying the pattern matching procedure to these optical images, it is found that the suspended beams do not exhibit any rotation. This result implies that the structural films on both the chips A and B do not have any residual stress in them, as expected. Also, as expected, the OTS SAM coating does not induces any stress in the Si(100) structural film, which is an indication that either the OTS SAM coating is conformal and uniform or it does not have any significant influence on the stress state of the structural Si(100) film.

On each of the two chips A and B, 16 MST's are tested. The width of each of the tested beams is determined optically to be 3.76 μm (design width is 4 μm). Table 1 lists the displacement at fracture of the tested beams along with the strain at fracture in the tested beams. Each reported value is an average of 16 data points. The mean values reported in Table 1 indicate that consistent results are obtained irrespective of the length of the tested beam. Also, as expected, the OTS SAM coating does not change the fracture strength of the Si(100) structural layer. The results obtained from both chip A and chip B are in good agreement with the values of fracture strength reported for Si(100) films in literature [12–15].

Seven resonators, each having a different folded suspension beam length are used to determine the Young's modulus (E) of the structural film on chip B. Table 2 lists the folded suspension beam lengths along with the corresponding observed resonance frequencies of the seven resonators used. Each resonance frequency reported in Table 2 is an average of three data points collected using three distinct resonators with same folded suspension beam lengths. By fitting the rearranged form of the Rayleigh equation given by Eq. 4 to the values reported in Table 2, the value of E for the structural film on chip B can be extracted. The slope of the fit shown in Fig. 7 (i.e., 129 GPa), which is the experimentally obtained value of E for the structural film on chip B, is in good agreement with that of a Si(100) film published in literature (i.e., 130 GPa) [9].

5.2 Adhesion

Four CBA's consisting of ten beams each are actuated on both chips A and B to determine the apparent work of adhesion between in-plane surfaces. The experiments are conducted in laboratory air at room temperature (i.e. 22°C) and a relative humidity (RH) of 13%. In-plane apparent work of adhesion reported in Table 3 for both the surface treatments are higher than those reported by Ashurst et. al. [6, 7]. Even though their experiments were conducted at a higher RH of 50%, they reported a lower in-plane apparent work of adhesion of 0.012 mJ/m^2 and 13.1 mJ/m^2 for OTS coated polysilicon surfaces and polysilicon surfaces with only native oxide on them respectively. The high $\mathcal{W}_{ip}$ exhibited by in-plane surfaces of both chip A and chip B even at a lower RH can be attributed to the smoother topography of the test surfaces of the TP reported in this paper as compared to the test surfaces used by Ashurst et. al. Two CBA's actuated on chip B under the same conditions except at a higher RH of 58% exhibited $\mathcal{W}_{ip}$ of 139 mJ/m^2. The apparent work of adhesion exhibited by the in-plane surfaces on chip B at high RH is very close to the theoretical limiting value of 144.96 mJ/m^2, which corresponds to 2γ, where γ is the surface tension of water (72.48 dynes/cm at 22 °C). This further substantiates the extremely smooth topography of the in-plane test surfaces of the TP reported

Beam Length (μm)	Displacement at Fracture $\delta_f \pm$ std.dev. (μm)		Strain at Fracture $\epsilon_f \pm$ std.dev. (%)	
	Chip A	Chip B	Chip A	Chip B
50	8.51 $\pm$ 0.49	8.48 $\pm$ 0.63	1.92 $\pm$ 0.11	1.91 $\pm$ 0.14
60	12.24 $\pm$ 1.24	12.30 $\pm$ 0.82	1.92 $\pm$ 0.19	1.93 $\pm$ 0.13
70	17.49 $\pm$ 0.39	17.48 $\pm$ 0.35	2.01 $\pm$ 0.05	2.01 $\pm$ 0.04

Table 1: Displacement at fracture of tested beams and strain at fracture tested beams on chip A and chip B

Supporting Beam Length (μm)	Resonance Frequency $f_R \pm$ std.dev. (KHz)
200	13.50 $\pm$ 0.01
250	9.15 $\pm$ 0.01
300	8.34 $\pm$ 0.01
350	6.14 $\pm$ 0.01
400	4.72 $\pm$ 0.01
450	3.92 $\pm$ 0.01
500	3.64 $\pm$ 0.01

Table 2: Resonance frequencies of resonators with different folded suspension beam lengths.

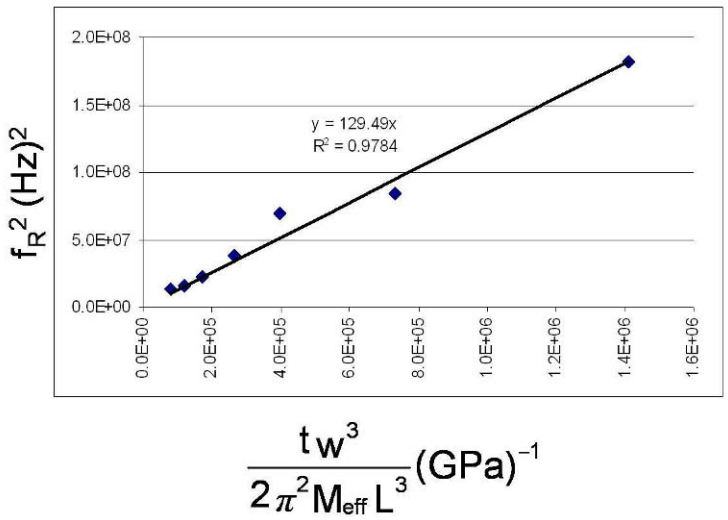

Figure 7: Plot exhibiting the fitting of Eq. 4 to the values reported in Table 2. The slope of the fitted line is the experimentally obtained value of E for the structural film on chip B.

in this paper. To determine the apparent work of adhesion between sidewall surfaces, two SBA's are actuated on both chip A and chip B in laboratory air at room temperature and a RH of 13%. Apparent work of adhesion between sidewall surfaces on both chip A and chip B as reported in Table 3 is less than that between the corresponding in-plane surfaces. This substantiates the role of roughness in reducing adhesion, since the sidewall surfaces (rms roughness is 6.52 nm) on both the chips have a rougher topography than the corresponding in-plane surfaces (rms roughness is 0.097 nm).

Chip	Apparent In-plane Work of Adhesion $\mathcal{W}_{ip} \pm$ std.dev. (mJ/m^2) (RH = 13%)	Apparent Sidewall Work of Adhesion $\mathcal{W}_s \pm$ std.dev. (mJ/m^2) (RH = 13%)
A	0.02 $\pm$ 0.001	$<$0.04
B	22.92 $\pm$ 2.5	1.065 $\pm$ 0.07

Table 3: Adhesion energies between in-plane and sidewall surfaces on chip A and chip B.

5.3 Friction

All the experiments to determine the coefficients of static friction (μ_s) between sidewall surfaces are conducted in laboratory air at room temperature and a RH of 13%. Three SFAT's and three SFT's are actuated on both chip A and chip B. As seen in Table 4, for sidewall surfaces on both chip A and chip B, the static friction coefficients determined using both the SFAT and SFT are in good agreement. However, Ashurst et. al. reported static friction coeffcients of 0.07 $\pm$ 0.005 and 1.1 $\pm$ 0.1 for OTS coated surfaces and surfaces with only native oxide on them respectively [6]. The

lower μ_s reported by Ashurst et. al could be attributed to the rougher topography of the polysilicon sidewall surfaces (rms roughness is 13.8 nm) of their test devices in comparison to the sidewall surfaces (rms roughness is 6.52 nm) of the TP reported in this paper. On the contrary, in-plane static friction coefficients of 0.09 ± 0.01 and 2.3 ± 0.8 for OTS coated polysilicon surfaces (rms roughness is 5 nm) and polysilicon surfaces having only native oxide on them (rms roughness is 5 nm) respectively, reported by Srinivasan et. al. are in good agreement with the sidewall static friction coefficients determined using the TP reported in this paper [5]. These results clearly emphasize the role of roughness in friction between contacting surfaces.

Chip	$\mu_s \pm$ std.dev.	
	SFAT	SFT
A	0.17 ± 0.03	0.15 ± 0.02
B	1.98 ± 0.4	1.69 ± 0.3

Table 4: Coefficients of static friction between sidewall surfaces (rms roughness is 6.52 nm) of chip A and chip B determined using both SFAT and SFT.

6. Conclusions

We designed a single mask scheme for facile and inexpensive fabrication of a micromachine test platform, which enables the test platform to be built in different types of structural layers. The test platform is successfully fabricated and shown to be a versatile tool that enables systematic investigations of several tribological properties. The micromachined surfaces of the test platform are the smoothest test surfaces used to-date. This attribute of the test platform can be used to systematically investigate the effects of roughness and topography on tribological properties by tailoring the roughness and topography of the test surfaces. The test platform is an ideal stage for testing and comparing the various strategies that can be used to address the tribological issues that are presently plaguing the MEMS community.

7. Acknowledgments

The authors wish to thank the Electrical & Computer Engineering department at Auburn university for allowing them to use the AMSTC facilities to fabricate the test platform. The authors also gratefully acknowledge the financial support of Auburn University.

References

[1] L. Phinney, G. Lin, J. Wellman, A. Garcia, Surface roughness measurements of micromachined polycrystalline silicon films, Journal of Micromechanics and Microengineering, 14, 927–931, 2004.

[2] R. Alley, G. Cuan, R. Howe, K. Komvopoulos, The effect of release etch processing on surface microstructure stiction, In Proc. of IEEE Solid State Sensor and Actuator Workshop, Hilton Head '92, 202–207, 1992.

[3] M. P. de Boer, T. A. Michalske, Accurate method for determining adhesion of cantilever beams, Journal of Applied Physics, 86 (2), 817–827, 1999.

[4] W. R. Ashurst, M. P. de Boer, C. Carraro, R. Maboudian, An investigation of sidewall adhesion in MEMS, Applied Surface Science, 212, 735–741, 2003.

[5] U. Srinivasan, J. Foster, U. Habib, R. T. Howe, R. Maboudian, D. Senft, M. Dugger, Lubrication of polysilicon micomechanisms with self-assembled monolayers, In Proc. of the 1998 Solid - State Sensor and Actuator Workshop, Hilton Head '98, 156–161, 1998.

[6] W. R. Ashurst, C. Yau, C. Carraro, R. Maboudian, M. T. Dugger, Dichlorodimethylsilane as an anti-stiction monolayer for MEMS: A comparison to the octadecyltrichlosilane self-assembled monolayer, Journal of Microelectromechanical Systems, 10 (1), 41–49, 2001.

[7] W. R. Ashurst, C. Carraro, R. Maboudian, W. Frey, Wafer level anti-stiction coatings for MEMS, Sensors and Actuators A-physical, 104 (3), 213–221, 2003.

[8] M. de Boer, T. Mayer, Tribology of MEMS, MRS Bulletin, 302–304, 2001.

[9] B. D. Jensen, M. P. de Boer, N. D. Masters, F. Bitsie, D. A. LaVan, Interferometry of actuated microcantilevers to determine material properties and test structure nonidealities in mems, Journal of Microelectromechanical Systems, 10 (3), 336–346, 2001.

[10] K. M. Hurst, C. B. Roberts, W. Ashurst, A New Method to Determine Adhesion of Cantilever Beams Using Beam Height Experimental Data, Tribology Letters, 35, 9–15, 2009.

[11] S. J. Timpe, K. Komvopoulos, Microdevice for measuring friction and adhesion properties of sidewall contact interfaces of Micro-electromechanical Systems, Review of Scientific Instruments, 78 (6), 065106, 2007.

[12] C. Chen, M. Leipold, Fracture toughness of silicon, Ceramic Bulletin, 59 (4), 1980.

[13] J. F. Nye, Physical Properties of Crystals, Oxford University Press, Oxford, 1985.

[14] R. Ballarini, R. L. Mullen, Y. Yin, H. Kahn, S. Stemmer, A. H. Heuer, The fracture toughness of polysilicon microdevices: A first report, Journal Of Materials Research, 12 (4), 915–922, 1997.

[15] H. Kahn, N. Tayebi, R. Ballarini, R. L. Mullen, A. H. Heuer, Fracture toughness of polysilicon mems devices, Sensors And Actuators A-Physical, 82 (1-3), 274–280, 2000.